

A new small satellite sunspot triggering recurrent standard- and blowout-coronal jets
YUHU MIAO,^{1,2,3,4,5,6} Y. LIU,^{1,2,3,4,5} Y. D. SHEN,^{1,2} A. ELMHAMDI,³ A. S. KORDI,³
H. B. LI,^{1,6} Z. Z. ABIDIN,⁴ AND Z. J. TIAN⁵

¹*Yunnan Observatories, Chinese Academy of Sciences, Kunming 650216, China*

²*Key Laboratory of Geospace Environment, Chinese Academy of Sciences, University of Science & Technology of China, Hefei 230026, China*

³*Department of Physics and Astronomy, King Saud University, PO Box 2455, Riyadh 11451, Saudi Arabia*

⁴*Radio Cosmology Lab, Department of Physics, Faculty of Science, University of Malaya, 50603 Kuala Lumpur, Malaysia.*

⁵*Institute of Space Physics, Luoyang Normal University, Luoyang, China*

⁶*University of Chinese Academy of Sciences, Beijing 100049, China*

(Accepted April 8, 2019)

ABSTRACT

In this paper, we report a detailed analysis of recurrent jets originated from a location with emerging, canceling and converging negative magnetic field at the east edge of NOAA active region AR11166 from 2011 March 09 to 10. The event presented several interesting features. First, a satellite sunspot appeared and collided with a pre-existing opposite polarity magnetic field and caused a recurrent solar jet event. Second, the evolution of the jets showed blowout-like nature and standard characteristics. Third, the satellite sunspot exhibited a motion toward southeast of AR11166 and merged with the emerging flux near the opposite polarity sunspot penumbra, which afterward, due to flux convergence and cancellation episodes, caused recurrent jets. Fourth, three of the blowout jets associated with coronal mass ejections (CMEs), were observed from field of view of the *Solar Terrestrial Relations Observatory*. Fifth, almost all the blowout jet eruptions were accompanied with flares or with more intense brightening in the jet base region, while almost standard jets did not manifest such obvious feature during eruptions. The most important, the blowout jets were inclined to faster and larger scale than the standard jets. The standard jets instead were inclined to relative longer-lasting. The obvious shearing and twisting motions of the magnetic field may be interpreted as due to the shearing and twisting motions for a blowout jet eruption. From the statistical results, about 30% blowout jets directly developed into CMEs. It suggests that the blowout jets and CMEs should have a tight relationship.

Keywords: Sun: activity — Sun: activity — Sun: — flares — Sun: magnetic fields — Sun: coronal mass ejections (CMEs)

1. INTRODUCTION

Solar jet activities are very common phenomena associated with magnetic flux emergence and cancellation. They are observed both in cool and hot plasma ejections from the photosphere to the outer corona in the solar atmosphere. Until to-date, many kinds of jet activities have been observed in different spectral lines, such as H α surges (Roy 1973; Liu & Kurokawa 2004; Jiang et al. 2007), extreme ultraviolet (EUV) (Shen et al. 2012; Li et al. 2015; Liu et al. 2015; Shen et al. 2011; Nisticò et al. 2015; Kumar et al. 2017; Zhu et al. 2017; Tian et al. 2017, 2018) and X-ray jets (Shibata et al. 1992; Vasheghani Farahani et al. 2009; Moore et al. 2010, 2013; Pucci et al. 2013; Sterling et al. 2015; Moore et al. 2018). Many researches indicated that most solar jets result from magnetic reconnection in the low solar atmosphere (Shibata et al. 1992, 1994; Canfield et al. 1996; Shimojo et al. 1996, 1998; Liu & Zhang 2002; Jiang et al. 2007; Shen et al. 2011; Hong et al. 2011; Shen et al. 2014; Li et al. 2015; Liu et al. 2015; Sterling et al. 2015; Li et al. 2015; Xu et al. 2016; Hong et al. 2017; Shen et al. 2017, 2012; Adams et al. 2014; Schmieder et al. 2015; Yang et al. 2016; Tian et al. 2018; Li et al. 2019; Panesar et al. 2018; Cheng et al. 2018). In the past few decades, numerous characteristics of the solar jets were found and summarized. According to Shimojo et al. (1996, 1998), the authors found that jets have the following features: 1) the general length is in the range of a few $\times 10^4$ to 4×10^5 km and the width is 5×10^3 to 10^5 km; 2) the lifetimes range from few minutes to more than ten hours; 3) the velocities are 10 km s^{-1} to 1000 km s^{-1} , and the average velocity is about 200 km s^{-1} ; 4) 72% of them happened at the mixed polarity regions. Liu et al. (2005b) reported a detailed analysis of the relationship between jet and jet-like CME. The authors indicated that a large scale jet probably can produced a jet-like CME.

By examining many X-ray jets, Moore et al. (2010) divided them into two types: one is standard jet and one is non-standard jet, which is called blowout jet. In the classification, about two thirds of them are standard type and about one third of them are blowout type. The authors also indicated that a blowout jet has enough free energy to drive an ejective eruption, because the blowout jet has strongly shear or twist in the field core of the arch. But, according to Moore et al. (2013), the authors presented 54 polar X-ray jets. There were 32 blowout jets, 19 standard jets and 3 ambiguous jets, respectively. The number of the blowout jets has about twice as many as standard jets. However, according to Moore et al. (2010), the number of the standard jets twice over the blowout jets. Combining the two samples, the authors indicated that the percentage of the blowout jets and standard jets is closer to 50%-50%. Some researches argued that jets could result in coronal mass ejections (CMEs; Wang et al. 1998; Moore et al. 2001; Liu et al. 2005a; Moore & Sterling 2006; Liu 2008; Shen et al. 2012; Liu et al. 2015; Shen et al. 2017; Sterling 2018; Tiwari et al. 2018) and the erupting plasmoid can be observed in the corona (Moore & Sterling 2007; Liu 2008). Moore et al. (2010) also constructed a model to interpret the blowout jet. Blowout jets have tight association with small filament eruptions (Moore et al. 2010; Shen et al. 2012; Miao et al. 2018), and they usually accompany with flares during the eruptions. In the last few years, jet eruptions were reported to be associated with CMEs by Liu et al. (2011), Shen et al. (2012), Liu et al. (2015), Miao et al. (2018) based on the high spatial and temporal resolution of the *Solar Dynamics Observatory* (SDO; Pesnell et al. 2012).

Recurrent jets appear to often occurred in mixed polarity regions (Chen et al. 2015; Liu et al. 2016). Magnetic reconnection is supposed to play a major role in the triggering mechanism of the jets (Shibata et al. 1994). Magnetic flux emergences, convergences and cancellations are the

important features in recurrent jet eruptions, that habitually appear near the pre-existing ambient magnetic field (Jiang et al. 2007; Sterling et al. 2018). In addition, many observational facts suggested that some jet activities can directly or indirectly result in large-scale magnetic reconfigurations such as filament, loop eruptions (e.g., Jiang et al. 2008; Wang et al. 2016; Zheng et al. 2016; Miao et al. 2018; Shen et al. 2018c), CMEs, and EUV waves (Zheng et al. 2012, 2013; Su et al. 2015; Patsourakos & Vourlidas 2009; Yang et al. 2017; Shen et al. 2018a,b; Miao et al. 2019). It should be noted that Shen et al. (2012); Miao et al. (2018) presented a blowout jet eruption associated with simultaneous double-CME event. Blowout jet eruptions are considered as a very important solar phenomenon and usually generate narrow and bubble-like CMEs (Liu 2008; Shen et al. 2012; Zheng et al. 2013; Archontis & Hood 2013; Chen et al. 2015; Chandra et al. 2017; Miao et al. 2018). According to Yashiro et al. (2003) and Vourlidas et al. (2013), a CME with angular width $\leq 20^\circ$ is dubbed narrow CME.

In the present work we report an event occurred from 2011 March 09 11:00 UT to March 10 09:00 UT at the east periphery region of AR11166 close to the solar disk center. The series jets included both blowout-like and standard jets. Three CMEs were produced by the counterpart of the three blowout jets. The paper is organized as follows. In Section 2, the reduction of the instruments and data. In Section 3, the results are briefly listed. In the last section, the conclusions and discussions are presented.

2. INSTRUMENTS AND DATA SETS

The recurrent jets were observed by the Atmospheric Imaging Assembly (AIA; Lemen et al. 2012) on board the *SDO* captures full-disk images of the Sun up to $1.3 R_\odot$ in seven EUV channels and three UV-visible channels, whose temporal cadences are 12 s and 24 s, respectively, with a resolution of $0''.6 \text{ pixel}^{-1}$. Six EUV wavelength channels: 94, 131, 171, 193, 211 and 335 Å wavelengths are due to strong iron lines with temperature range from 0.6 MK to 16 MK. The 304 Å wavelength is due to He II line. In this paper, only 304 and 171 Å images are used to detect the jets. The line-of-sight (LOS) magnetograms and continuum intensity images were taken by the Helioseismic and Magnetic Imager (HMI; Scherrer et al. 2012) on board the *SDO*, whose temporal and spatial resolutions are 45 s and $0''.5$, respectively. The Space-weather HMI Active Region Patches (SHARPs; Bobra et al. 2014) are also used for displaying the vector magnetic field evolution. The jets were also observed by the Extreme Ultraviolet Imager (EUVI; Howard et al. 2008) of the Sun Earth Connection Coronal and Heliospheric Investigation (SECCHI; Howard et al. 2008) on board the *Solar TERrestrial Relations Observatory (STEREO; Kaiser et al. 2008)* providing full-disk He II 304 Å images, with a 5 and 10 minute cadences and a pixel width of $1''.6$. The three CMEs were captured by the inner coronagraphs (COR1) and the outer coronagraphs (COR2) on board the *STEREO/Ahead (STA)* and *STEREO/Behind (STB)*, whose cadences and field of views (FOVs) are 5 minutes, $1.4\text{--}4 R_\odot$ and $2.5\text{--}15.6 R_\odot$ (Thompson et al. 2003), respectively.

3. OBSERVATIONS AND DATA ANALYSIS

In defining and recognizing standard/blowout jets, Moore et al. (2010, 2013, 2015, 2018) assumed a relatively simple magnetic structure, with a single bipole embedded in a background unipolar magnetic field. Based on that, they defined “standard” and “blowout” jets based (in part) on the width of the spire compared to the size of the jet’s bipolar base, and based on observations in Hinode/XRT X-rays and AIA EUV images. Their setup was representative of the magnetic situation

for jets in coronal holes. The magnetic field at the base of our active region jets is much more complicated than the simplified situation of Moore et al.. Therefore we cannot define our jets as blowout or standard jets in exactly the same way that Moore et al. did. But, by looking at AIA EUV movies of the jets of our region, we found many of them to tend to have relatively narrow spires compared to the width of the negative patch shown in Figure 5(b), and others of them to have spires that grew to be comparable in width to that patch. Based on this, we classified the relatively-narrow-spire jets as standard jets, and the relatively-broad-spire jets as blowout jets. We expect that our so-determined standard and blowout jets fit closely with the categories defined by Moore et al..

Table 1 lists the blowout-like and standard jets from 2011 March 09 to 2011 March 10. The table includes thirty-seven jets. Many of them are standard jets (about 73% of the total statistical data), while the remaining events are blowout-like. The jets are observed through 171 and 304 Å wavelengths of the *SDO/AIA* in the study. The first column in the table displays the number of the jet events. The second and the third columns in the table show the detection time of the jets. The fourth column displays the flares associated with the jet eruptions. The fifth column reports the CMEs velocities from both COR2-A and COR2-B. The sixth column presents the speeds of the jets and the seventh column shows the duration time during the rise phase of the jets. The eighth column displays the lengths of the jets. We use the $1'' \approx 720 \text{ km}^a$. The ninth column shows the types of the jets. The “ST” and “BL” denote the standard jet and the blowout jet, respectively. The characteristics of the standard jet and blowout jet present several differences (Moore et al. 2010; Liu et al. 2011; Shen et al. 2012; Moore et al. 2013; Pucci et al. 2013; Sterling et al. 2016; Liu et al. 2016). A movie highlighting all the jet eruptions, made using 171 and 304 Å images (video1.mpeg) is given with the online accompanying material. It should be noted that some very small jets are excluded because they appear to be too blurred to be distinguished. The data at the beginning of the jet J11 is little blurred probably due to a little shake of the *SDO*.

Table 2 lists the details of the three CME events, observed by *STEREO/COR2-A* and *COR2-B*. The three CMEs were detected on March 09 18:24 UT, 23:54 UT and March 10 07:54 UT from *COR2-A*, respectively. On 2011 March 09 and 10, the separation angle between *STEREO/Ahead* (STA) and *STEREO/Behind* (STB) were about 177° , while that between STA (STB) and *SDO* was about 88° (95°). Worth to note that *STEREO/COR2-B* data did not observe the third CME, while the *STEREO/COR1-B* captured it (see Figure 7(b3)). In the table, we focus on the *COR2-A* observed results and list the *COR2-B* data only for reference. The CME events in Table 2 can be found on the page SECCHI-A and -B CME Lists¹ from *STEREO*. The seventh column displays the angular width of the three CMEs. According to Table 2, two CMEs angular widths are $\leq 20^\circ$. The two CMEs can be hence called narrow CMEs and they were triggered by the counterpart two blowout jet eruptions. Actually, all of the three CMEs were triggered by blowout jets. Interestingly, Miao et al. (2018) presented a double-CME event associated with the jet J15. The authors displayed a simultaneous jet-like CME and bubble-like CME eruption that was triggered by the jet J15 eruption. Hence strictly speaking, we observe four CMEs, three are jet-like CMEs and a one bubble-like CME. According to the CME angular width, the CMEs can be classified as three narrow CMEs and a bubble-like CME.

¹ <https://secchi.nrl.navy.mil/cactus/>

Figure 1 shows the speeds of the blowout and the standard jets. The red “*” symbol represents the speeds of the standard jets and the green “*” symbol represents the speeds of the blowout jets’, respectively. Combing with Table 1 and Figure 1, the blowout jets are faster and larger than the standard jets. According Moore et al. (2010), a blowout jet is more intense than a standard jet during the eruption stage. It should be noted that the three CMEs are triggered by the blowout jets. On the one hand, this might explain why the blowout jet is actually more intense. On the other hand, the blowout jet eruption tends to release large amounts of energy.

Interestingly, a satellite sunspot appeared near the main sunspot penumbra at about 11:30 UT. In Figure 2 panel (b), at about 12:00 UT, the satellite sunspot was easily distinguishable at the east edge of AR11166. Panel (a) shows the HMI LOS magnetic field of the small sunspot near the main pre-existing sunspot. Panels (c) and (d) illustrate the first jet using the *SDO/AIA* 171 and 304 Å, respectively. “J1” is the first jet in Table 1. After 14:00 UT, the satellite sunspot was moving toward the southeast of the edge of AR11166 with a very slow velocity. We measure the velocity of the satellite sunspot to be about 0.4 km s^{-1} (see the top row of Figure 3). Panels (a) to (d) of Figure 3 show the satellite sunspot evolution. Panels (e) to (h) of Figure 3 display the LOS magnetic field evolution from March 09 12:00 UT to March 10 00:00 UT. Later on, the magnetic field of the jet base gets more and more complex and the negative magnetic field became more intense. In order to display the satellite sunspot and the counterpart of magnetic field evolutions, we provide a movie (video2.mpeg; in the online journal), constructed using HMI continuum intensity images and LOS magnetograms.

Five jets are displayed in Figure 4. Panels (a) to (e) in the first column correspond to HMI LOS magnetograms highlighting evolution of the jet base region magnetic flux. Panels (f) to (j) in the second column are HMI continuum intensity images displaying the evolution of the satellite sunspot. The third and fourth columns are 171 and 304 Å images for the five jets. They counterpart with the magnetic flux evolution of the jet base region, which we report in the first and second columns. the other jets can be recognized in the online animation material: video1.mpeg. From the first and the second columns, the magnetic field evolution is very clear. Worth to mention here that we mainly focus on the negative flux evolution, because the pre-existing sunspot is too big to accurately measure the positive flux evolution.

In order to inspect the negative flux evolution of the jet base region, we measure data from March 09 11:00:30 UT to March 10 10:00:30 UT. The results are displayed in Figure 5. Panel (a) shows AR11166 with the box indicating the jet base region. The box region is shown in panel (b) of Figure 5. Panel (c) presents the evolution of the negative flux at jet base region. It is so important to pay more attention to the negative flux region. The positive flux region is too large and complex which impedes a precise quantification of the positive flux. The result suggests that the negative flux shows manifests both emergence and cancellation episodes during the whole stage. The overall trend indicates emergence to be more intense and faster than cancellation. It should be noted that the cancellation is undergoing on both the north and south sides of the negative patch, which near the pre-existing positive polarity. Actually, the jets come from both of these locations. Sterling et al. (2017) indicated that eruptions of strong jets occur only during times of intense flux cancellation. Our observations are consistent with this, because our jets come from the two locations where we see cancellation.

According to Yang et al. (2013) and Chen et al. (2015), the jets are usually produced by the magnetic reconnection or cancellation. In order to understand the evolution of the satellite sunspot and magnetic field, we analyze vector magnetograms around the jet region. In Figure 6, the roman numerals “I”, “II”, “III”, represent the satellite sunspot flux region, emergence flux region and the whole of the jet base region, respectively. To distinctly scrutinize the vector magnetic flux evolution, we present a movie (video3.mpeg) of the evolution of the magnetic field of the jet base region. From video3.mpeg, we could easily observe the evolution of the vector magnetic flux in the jet base region. The satellite sunspot moved towards the southeast of the pre-existing sunspot and merged with the emergence flux from March 09 to March 10. The video3.mpeg also displays characteristics of strong twisting motion and shearing motion of the magnetic field at the jet base region.

During the time interval March 09 11:00 UT to March 10 08:00 UT, there were three large scale CMEs produced by blowout jet eruption. The details of the three CMEs are listed in Table 1 and Table 2, which are observed from the *STEREO*/COR2. In Figure 7 we display the three CMEs. Snapshots are 304 Å and running difference COR1 images at the limb as viewed from *STEREO* Ahead and Behind.

Figure 7 reports the composite EUVI 304 Å and COR1 images. The structures of the three CMEs can be clearly seen. Panels (a1), (b1) show the first CME at about 17:40 UT. Panels (a2), (b2) display the second CME, which is a double-CME event (see Miao et al. (2018) for more details). Panels (a3), (b3) present the third CME. The three CMEs have a common characteristic namely being triggered by the blowout jets.

4. CONCLUSIONS AND DISCUSSIONS

The solar recurrent jets occurring from 2011 Mach 09 12:00 UT to 2011 March 10 08:00 UT have been investigated in the present work. The jets can be classified into two types, namely, blowout jet and standard jet. We mainly focus on the recurrent jets and three CMEs associated with blowout jets. The main observational results can be summarized as follows.

1. The recurrent jet eruption associated with a newly formed satellite sunspot, together with a negative flux appeared in the penumbra of the main sunspot at about 11:30 UT on March 09. After 14:00 UT, the penumbra southeast of AR11166, presents a scenario whereby the negative pole of an emerging-flux element is growing in a sea of positive polarity. We measure the speed of the small satellite sunspot to be 0.4 km s^{-1} .

2. During the whole process, ten blowout jets and twenty-seven standard jets were observed. About 27% are the blowout jets while 73% belong to standard jets.

3. All the blowout jet velocities are found to be larger than those of standard jets. We report the velocity results in Table 1. Compared to standard jets, blowout jets are generally brighter and more explosive in EUV, suggesting that they are undergoing intense magnetic reconnection. This may suggest that the blowout jet releases more energy than standard jets.

4. The eruption processes of magnetic cancellation and emergence are clearly identified and reported. From the video2.mpeg and the video3.mpeg, we can evidently recognize the magnetic field evolution at the the jet base region. Many new small emerging fluxes collided and converged during the whole stage. Especially, the obvious shearing and twisting motions of the magnetic field are probably interpreted as indication of the shearing and twisting motions for blowout jet eruptions. When a blowout jet erupted, the shearing and twisting motions of the magnetic field (see the video2.mpeg and video3.mpeg) appear more intense than a standard jet.

Table 1. Date and time for the observed jets, and their measured parameters.

Jets:								
Jet No.	Date	Time (UT)	Flare class	CME Speed (km s ⁻¹)	Jet Speed (km s ⁻¹)	Jet Rise Dur. (± 1 min)	Jet Length ^a (± 1500 km)	Type ST or BL ^b
J1	09-Mar-11	11:59:08	92	13	72000	ST
J2	09-Mar-11	12:07:32	55	13	43200	ST
J3	09-Mar-11	12:45:56	40	15	36000	ST
J4	09-Mar-11	13:40:32	39	20	46700	ST
J5	09-Mar-11	14:05:08	44	15	39600	ST
J6	09-Mar-11	14:15:20	72	10	43200	ST
J7	09-Mar-11	14:30:20	42	17	43200	ST
J8	09-Mar-11	15:27:20	50	18	50400	ST
J9	09-Mar-11	16:55:32	...	256 ^c , 126 ^d	156	23	216000	BL
J10	09-Mar-11	19:00:20	120	15	108000	ST
J11	09-Mar-11	19:15:53	184	13	144000	BL
J12	09-Mar-11	19:50:08	135	16	129600	ST
J13	09-Mar-11	20:37:32	70	26	108000	ST
J14	09-Mar-11	21:05:08	200	18	216000	BL
J15	09-Mar-11	22:05:08	C9.4 ^e	337 ^f , 143 ^g	350 ^h	25	435000	BL
J16	09-Mar-11	23:48:20	100	12	72000	ST
J17	10-Mar-11	00:28:32	145	12	104400	ST
J18	10-Mar-11	01:00:20	120	15	108000	ST
J19	10-Mar-11	01:30:20	138	10	108000	ST
J20	10-Mar-11	01:40:32	140	9	75600	ST
J21	10-Mar-11	01:49:32	175	12	126000	BL
J22	10-Mar-11	02:51:20	135	12	97200	ST
J23	10-Mar-11	02:53:08	133	11	72000	ST
J24	10-Mar-11	03:06:56	193	13	151200	BL
J25	10-Mar-11	03:30:20	92	13	72000	ST
J26	10-Mar-11	03:45:20	120	10	72000	ST
J27	10-Mar-11	04:05:08	C2.9 ⁱ	-	165	12	118000	BL
J28	10-Mar-11	04:23:08	129	15	116000	ST
J29	10-Mar-11	04:43:32	129	15	116000	ST
J30	10-Mar-11	04:50:08	150	10	90000	ST
J31	10-Mar-11	05:41:08	96	10	57600	ST
J32	10-Mar-11	06:08:08	125	13	97200	ST
J33	10-Mar-11	06:19:32	150	12	108000	ST
J34	10-Mar-11	06:30:56	135	8	64800	ST
J35	10-Mar-11	06:41:08	...	263 ^j	158	19	180000	BL
J36	10-Mar-11	07:53:08	168	5	50400	BL
J37	10-Mar-11	07:59:08	168	5	50400	BL

^aWe use the 1 arcsec \approx 720km

^bBL means Blowout and ST means Standard, respectively.

^c<https://secchi.nrl.navy.mil/cactus/index.php?p=SECCHI-A/2011/03/out/Flow0005/CME.html>

^d<https://secchi.nrl.navy.mil/cactus/index.php?p=SECCHI-B/2011/03/out/Flow0009/CME.html>

^e<https://www.solarmonitor.org/?date=20110309>

^f<https://secchi.nrl.navy.mil/cactus/index.php?p=SECCHI-A/2011/03/out/CME0032/CME.html>

^g<https://secchi.nrl.navy.mil/cactus/index.php?p=SECCHI-B/2011/03/out/CME0030/CME.html>

^hSee the velocity in the paper [Miao et al. \(2018\)](#)

ⁱ<https://www.solarmonitor.org/?date=20110310>

^j<https://secchi.nrl.navy.mil/cactus/index.php?p=SECCHI-A/2011/03/out/CME0034/CME.html>

5. The three CMEs were produced by the corresponding blowout jet eruptions. All of the jets are displayed in Table 1, where the jet J15 has the largest scale. This blowout jet led to a double-CME event ([Miao et al. 2018](#)). Blowout jets were easily observed in the region of the recurrent jets, with distinct complex magnetic field and mixed polarities. From the statistical results, about 30% blowout jets directly developed into CMEs. Due to the low resolution of the *STEREO*, we consider that is probably more than 30% blowout jets can directly developed into CMEs. The forecast requires of course more statistical data to be confirmed in the future.

Table 2. Date and time for the observed jets, and their measured parameters.

CME-producing Jets:								
Jet No.	CME No.	Date	Time (UT)	Flare Class	CME Speed (km s ⁻¹)	CME Angular Width (°)	CME Rise Dur. (hour)	Jet Type
J9	cme1a ^c	09-Mar-11	18:24	...	256	20	01	BL
J15	cme2a ^f	09-Mar-11	23:54	C9.4 ^e	337	44	03	BL
J35	cme3a ^j	10-Mar-11	07:54	...	263	14	01	BL
Jet No.	CME No.	Date	Time (UT)	Flare Class	CME Speed (km s ⁻¹)	CME Angular Width (°)	CME Rise Dur. (hour)	Jet Type
STEREO/COR2-B								
J9	cme1b ^d	09-Mar-11	18:24	...	126	16	00	BL
J15	cme2b ^g	09-Mar-11	23:24	C9.4 ^e	143	24	01	BL
J35	...	10-Mar-11	BL

In Table 1, ten blowout jet eruptions and twenty-seven standard jet eruptions were observed from 2011 March 09 to March 10. According to Moore et al. (2010), the authors observed the interior base arch brightened with the production of the blowout jet. They thought that in blowout jet the interior of the base arch takes part in the eruption. According to the video1.mpeg, all of the blowout jets brightened in the interior of the base arch with the blowout jet eruptions. The brightening in the interior of the base arch becomes more extensive. In Table 1 and Table 2, two large blowout jet eruptions are associated with C class flares.

The magnetic emergence and cancellation both play an important role in this jet activities. There are few events associated with a new sunspot triggering the recurrent jet events. Interestingly, the new satellite sunspot appears to move toward the emergence region in the southeast of the main sunspot. The satellite sunspot had negative flux as the same emergence flux. At about 21:00 UT on March 09, the satellite sunspot and the emergence flux converged together. From Figure 6, during the evolution of the vector magnetic, the jet base region had intense cancellation (see video2.mpeg; material online). It suggests that the jet base region embodies very intense flux emergence feature. The negative flux evolution indicates that the emergence, cancellation and convergence co-exist at the same time. Through all the study stage, the emergence appears more intense than the cancellation.

According to Moore et al. (2010); Wang & Liu (2010); Chen et al. (2015), the eruption of blowout jet requires a large amount of energy. From the video1.mpeg and Table 1, we can see that the blowout jet eruptions accompany the brightening in the jet base region at the beginning. The jet J15 eruption accompanied with the C9.4 flare was observed at about 22:05 UT. In Table 1, the scale of most of blowout jets are larger than standard jets and the velocities are faster than standard jets (Pucci et al. 2013). The results indicate that a blowout jet eruption need more energy than a standard jet. Liu et al. (2016); Pucci et al. (2013) reported that during the magnetic reconnection of blowout jet more free energy should be released compared to standard jets. It suggested that the scale of a blowout jet should be usually larger than a standard jet. According to Figure 6 and video3.mpeg, magnetic emergence and cancellation were clearly very intense. We believe that cancellation has provide enough amount of energy to keep the recurrent jet eruptions. Even some blowout jet eruptions can produce CMEs, such as jet J9, J15 and J35 in the listed in Table 1 and Table 2. Liu (2008) has studied the relationship between surges and CMEs. Due to the low cadence of the data in Liu (2008), we considered that the jet-like surges probably are blowout jets. The narrow CMEs were formed directly from the blowout jet eruptions. In addition and according to Liu (2008); Moore et al. (2010) and Table 1, 2, The statistical results support that the blowout

jets and CMEs have a tight relationship. Our results therefore might suggest that a blowout jet has larger scale and needs more free magnetic reconnection energy than a standard jet. More similar observational investigations will be reported to confirm and support our present findings in the future.

In this paper, we reported the finding of thirty-seven jets and three CMEs as displayed in Table 1 and Table 2. Our study suggests that the blowout or blowout-like jets are larger and faster than the standard jets. Another intriguing result indicates that the blowout type eruptions can more easily trigger CMEs than standard type. The blowout jet eruptions tend to be accompanied with more intense flares or brightenings. We believe many new characteristics can be reported from recurrent jet eruptions in the future, which may aide to promote hence the development of new physical aspects of these interesting events.

We are grateful to the *SDO* and *STEREO* teams for the excellent data they provided. We also thank the referee for valuable suggestions and comments that improved the quality of this paper. This work is funded by the grants from the Strategic Priority Research Program of CAS with grant XDA-17040507, the National Scientific Foundation of China (NSFC 11533009, 11773068) and from the Key Laboratory of Geospace Environment, CAS, University of Science and Technology of China. This work is also supported by the grant associated with project of the Group for Innovation of Yunnan Province. The authors Y. Liu and Z.Z. Abidin would like to thank the University of Malaya Faculty of Science grant (GPF040B-2018) for their support. The authors extend their appreciation to the Deanship of Scientific Research at King Saud University for funding this work through research group No. (RG-1440-092). In addition, we are also grateful to the One Belt and One Road project of the West Light Foundation, CAS.

REFERENCES

- Adams, M., Sterling, A. C., & Moore, R. L. 2014, in AGU Fall Meeting Abstracts, Vol. 2014, SH51C-4178
- Archontis, V., & Hood, A. W. 2013, ApJ, 769, L21
- Bobra, M. G., Sun, X., Hoeksema, J. T., et al. 2014, SoPh, 289, 3549
- Canfield, R. C., Reardon, K. P., Leka, K. D., et al. 1996, ApJ, 464, 1016
- Chandra, R., Mandrini, C. H., Schmieder, B., et al. 2017, A&A, 598, A41
- Chen, J., Su, J., Yin, Z., et al. 2015, ApJ, 815, 71
- Cheng, X., Li, Y., Wan, L. F., et al. 2018, ApJ, 866, 64
- Hong, J., Jiang, Y., Yang, J., Li, H., & Xu, Z. 2017, ApJ, 835, 35
- Hong, J., Jiang, Y., Zheng, R., et al. 2011, ApJL, 738, L20
- Howard, R. A., Moses, J. D., Vourlidas, A., et al. 2008, SSRv, 136, 67
- Jiang, Y., Shen, Y., Yi, B., Yang, J., & Wang, J. 2008, ApJ, 677, 699
- Jiang, Y. C., Chen, H. D., Li, K. J., Shen, Y. D., & Yang, L. H. 2007, A&A, 469, 331
- Kaiser, M. L., Kucera, T. A., Davila, J. M., et al. 2008, SSRv, 136, 5
- Kumar, P., Nakariakov, V. M., & Cho, K.-S. 2017, ApJ, 836, 121
- Lemen, J. R., Title, A. M., Akin, D. J., et al. 2012, SoPh, 275, 17
- Li, X., Yang, S., Chen, H., Li, T., & Zhang, J. 2015, ApJL, 814, L13
- Li, X., Zhang, J., Yang, S., & Hou, Y. 2019, PASJ, 71, 14
- Liu, C., Deng, N., Liu, R., et al. 2011, ApJL, 735, L18
- Liu, J., Wang, Y., Shen, C., et al. 2015, ApJ, 813, 115
- Liu, J., Wang, Y., Erdélyi, R., et al. 2016, ApJ, 833, 150
- Liu, Y. 2008, SoPh, 249, 75
- Liu, Y., & Kurokawa, H. 2004, ApJ, 610, 1136

- Liu, Y., Kurokawa, H., Kitai, R., Ueno, S., & Su, J. T. 2005a, *SoPh*, 228, 149
- Liu, Y., Su, J. T., Morimoto, T., Kurokawa, H., & Shibata, K. 2005b, *ApJ*, 628, 1056
- Liu, Y., & Zhang, H. Q. 2002, *A&A*, 386, 646
- Miao, Y., Liu, Y., Li, H. B., et al. 2018, *ApJ*, 869, 39
- Miao, Y. H., Liu, Y., Shen, Y. D., et al. 2019, *ApJ*, 871, L2
- Moore, R. L., Cirtain, J. W., Sterling, A. C., & Falconer, D. A. 2010, *ApJ*, 720, 757
- Moore, R. L., & Sterling, A. C. 2006, in *Bulletin of the American Astronomical Society*, Vol. 38, AAS/Solar Physics Division Meeting #37, 247
- Moore, R. L., & Sterling, A. C. 2007, *ApJ*, 661, 543
- Moore, R. L., Sterling, A. C., & Falconer, D. A. 2015, *ApJ*, 806, 11
- Moore, R. L., Sterling, A. C., Falconer, D. A., & Robe, D. 2013, *ApJ*, 769, 134
- Moore, R. L., Sterling, A. C., Hudson, H. S., & Lemen, J. R. 2001, *ApJ*, 552, 833
- Moore, R. L., Sterling, A. C., & Panesar, N. K. 2018, *ApJ*, 859, 3
- Nisticò, G., Zimbardo, G., Patsourakos, S., Bothmer, V., & Nakariakov, V. M. 2015, *A&A*, 583, A127
- Panesar, N. K., Sterling, A. C., Moore, R. L., et al. 2018, *ApJ*, 868, L27
- Patsourakos, S., & Vourlidas, A. 2009, *ApJL*, 700, L182
- Pesnell, W. D., Thompson, B. J., & Chamberlin, P. C. 2012, *SoPh*, 275, 3
- Pucci, S., Poletto, G., Sterling, A. C., & Romoli, M. 2013, *ApJ*, 776, 16
- Roy, J. R. 1973, *SoPh*, 28, 95
- Scherrer, P. H., Schou, J., Bush, R. I., et al. 2012, *SoPh*, 275, 207
- Schmieder, B., Aulanier, G., & Vršnak, B. 2015, *SoPh*, 290, 3457
- Shen, Y., Ichimoto, K., Ishii, T. T., et al. 2014, *ApJ*, 786, 151
- Shen, Y., Liu, Y., Liu, Y. D., et al. 2018a, *ApJ*, 861, 105
- Shen, Y., Liu, Y., Su, J., & Deng, Y. 2012, *ApJ*, 745, 164
- Shen, Y., Liu, Y., Su, J., & Ibrahim, A. 2011, *ApJL*, 735, L43
- Shen, Y., Liu, Y. D., Su, J., Qu, Z., & Tian, Z. 2017, *ApJ*, 851, 67
- Shen, Y., Tang, Z., Li, H., & Liu, Y. 2018b, *MNRAS*, 480, L63
- Shen, Y., Tang, Z., Miao, Y., Su, J., & Liu, Y. 2018c, *ApJL*, 860, L8
- Shibata, K., Nitta, N., Strong, K. T., et al. 1994, *ApJL*, 431, L51
- Shibata, K., Ishido, Y., Acton, L. W., et al. 1992, *PASJ*, 44, L173
- Shimojo, M., Hashimoto, S., Shibata, K., et al. 1996, *PASJ*, 48, 123
- Shimojo, M., Shibata, K., & Harvey, K. L. 1998, *SoPh*, 178, 379
- Sterling, A. C. 2018, in *Journal of Physics Conference Series*, Vol. 1100, *Journal of Physics Conference Series*, 012024
- Sterling, A. C., Moore, R. L., Falconer, D. A., & Adams, M. 2015, *Nature*, 523, 437
- Sterling, A. C., Moore, R. L., Falconer, D. A., et al. 2016, *ApJ*, 821, 100
- Sterling, A. C., Moore, R. L., Falconer, D. A., Panesar, N. K., & Martinez, F. 2017, *ApJ*, 844, 28
- Sterling, A. C., Moore, R. L., & Panesar, N. K. 2018, *ApJ*, 864, 68
- Su, W., Cheng, X., Ding, M. D., Chen, P. F., & Sun, J. Q. 2015, *ApJ*, 804, 88
- Thompson, W. T., Davila, J. M., Fisher, R. R., et al. 2003, in *Proc. SPIE*, Vol. 4853, *Innovative Telescopes and Instrumentation for Solar Astrophysics*, ed. S. L. Keil & S. V. Avakyan, 1–11
- Tian, Z., Liu, Y., Shen, Y., et al. 2017, *ApJ*, 845, 94
- Tian, Z., Shen, Y., & Liu, Y. 2018, *NewA*, 65, 7
- Tiwari, S. K., Moore, R. L., De Pontieu, B., et al. 2018, *ApJ*, 869, 147
- Vasheghani Farahani, S., Van Doorselaere, T., Verwichte, E., & Nakariakov, V. M. 2009, *A&A*, 498, L29
- Vourlidas, A., Lynch, B. J., Howard, R. A., & Li, Y. 2013, *SoPh*, 284, 179
- Wang, H., & Liu, C. 2010, *ApJL*, 716, L195
- Wang, R., Liu, Y. D., Zimovets, I., et al. 2016, *ApJL*, 827, L12
- Wang, Y.-M., Sheeley, Jr., N. R., Socker, D. G., et al. 1998, *ApJ*, 508, 899
- Xu, Z., Jiang, Y., Yang, J., Yang, B., & Bi, Y. 2016, *ApJL*, 820, L21
- Yang, B., Jiang, Y., Yang, J., Yu, S., & Xu, Z. 2016, *ApJ*, 816, 41

- Yang, L., Yan, X., Li, T., Xue, Z., & Xiang, Y. 2017, *ApJ*, 838, 131
- Yang, L., Zhang, J., Liu, W., Li, T., & Shen, Y. 2013, *ApJ*, 775, 39
- Yashiro, S., Gopalswamy, N., Michalek, G., & Howard, R. A. 2003, *Advances in Space Research*, 32, 2631
- Zheng, R., Chen, Y., Du, G., & Li, C. 2016, *ApJL*, 819, L18
- Zheng, R., Jiang, Y., Yang, J., et al. 2013, *ApJ*, 764, 70
- . 2012, *ApJL*, 753, L29
- Zhu, X., Wang, H., Cheng, X., & Huang, C. 2017, *ApJL*, 844, L20

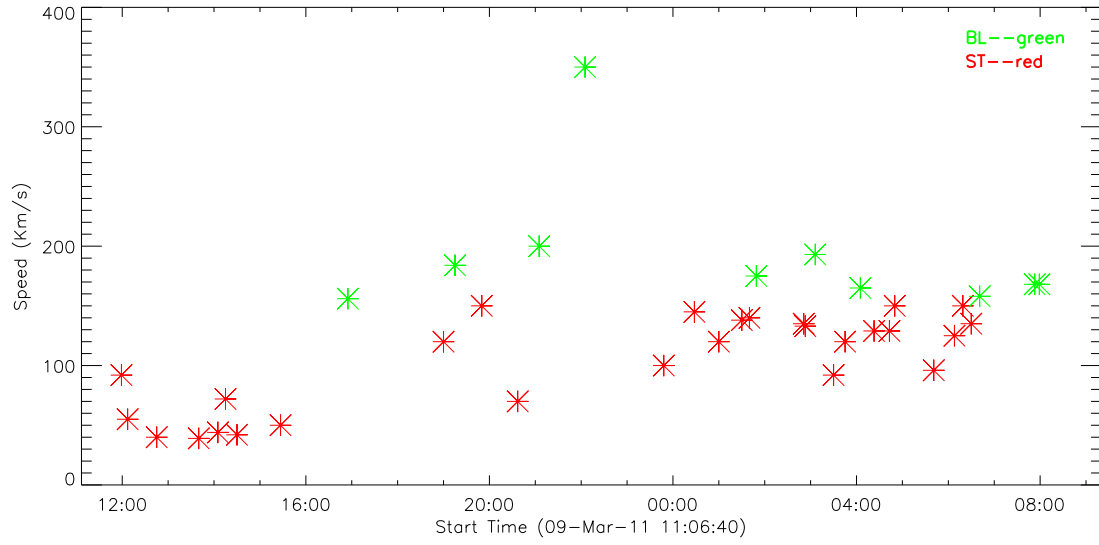


Figure 1. The two type jets velocities evolutions. The red “*” represents standard jets and the green “*” represents blowout jets, respectively.

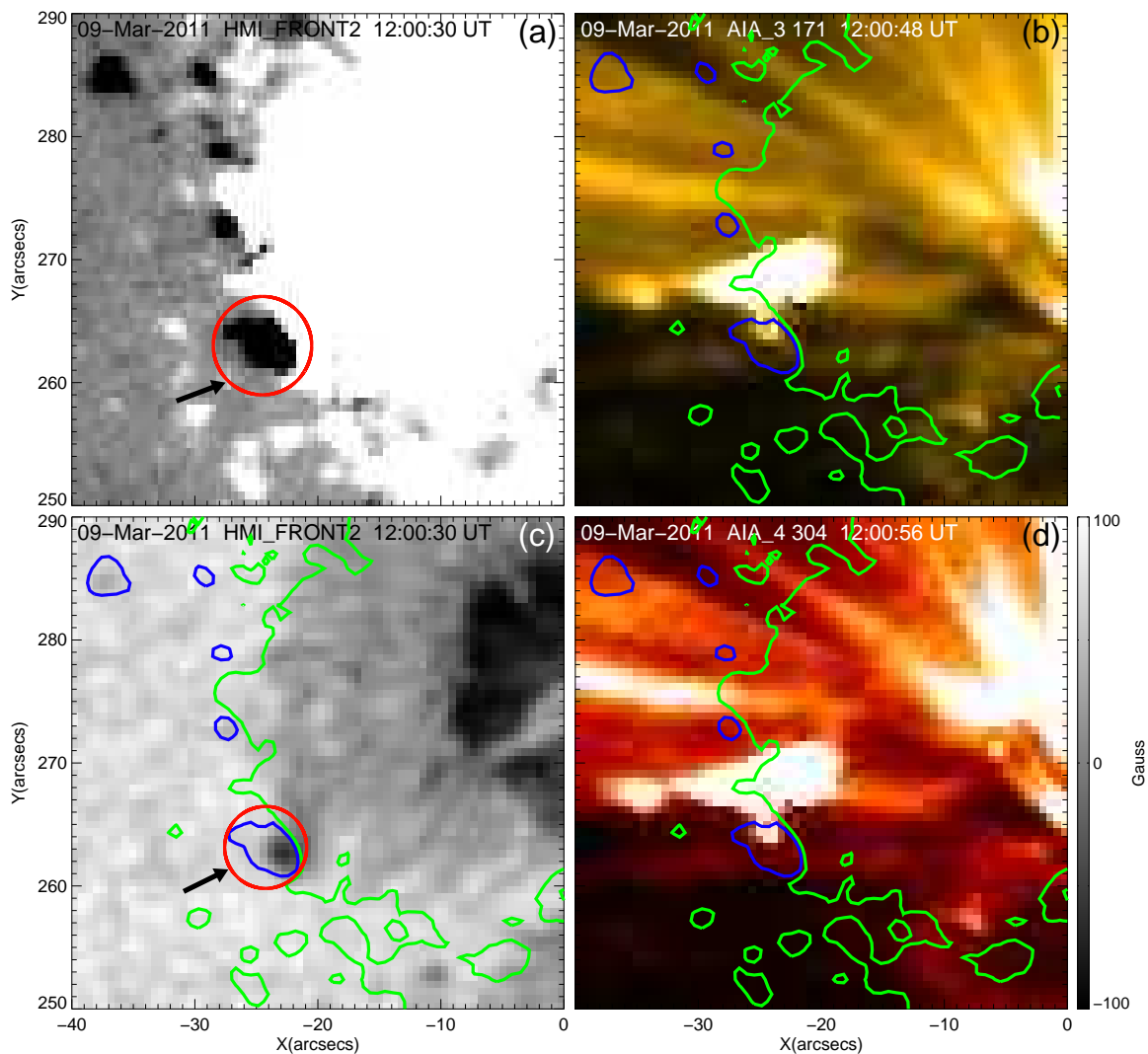


Figure 2. Panels (a) and (c) display the HMI magnetogram and HMI continuum intensity image, respectively. Panels (c), (b), and (d) show the contour levels ± 100 G. The blue and green lines represent negative and positive flux, respectively. The red circles encompass regions highlighting the small sunspot in panel (a) and the corresponding magnetic field in panel (c). Panels (b) and (d) show the first jet (J1) at 171 \AA and 304 \AA , respectively.

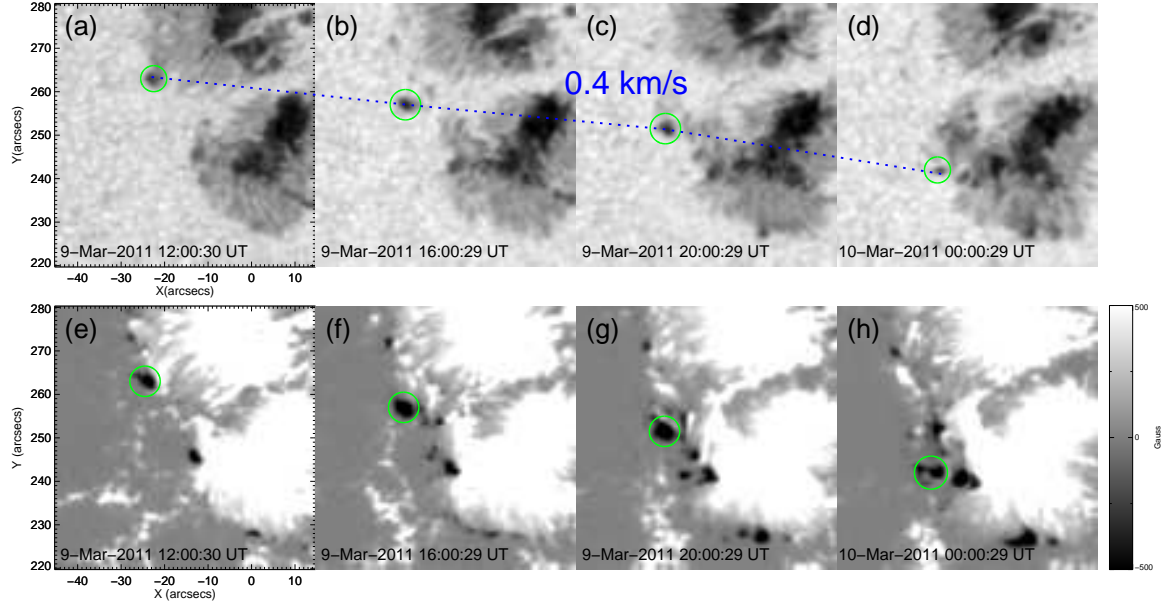


Figure 3. A set of *SDO/HMI* continuum intensity images displaying the satellite sunspot evolution and measured the moving average velocity to be about 0.4 km s^{-1} in the top row. The bottom row shows the magnetic field evolution using the *SDO/HMI* magnetograms. The green circle regions represent the small sunspot and the corresponding magnetic field in the two rows, respectively. The blue dotted lines highlight the satellite sunspot motion path (see video2.mpeg).

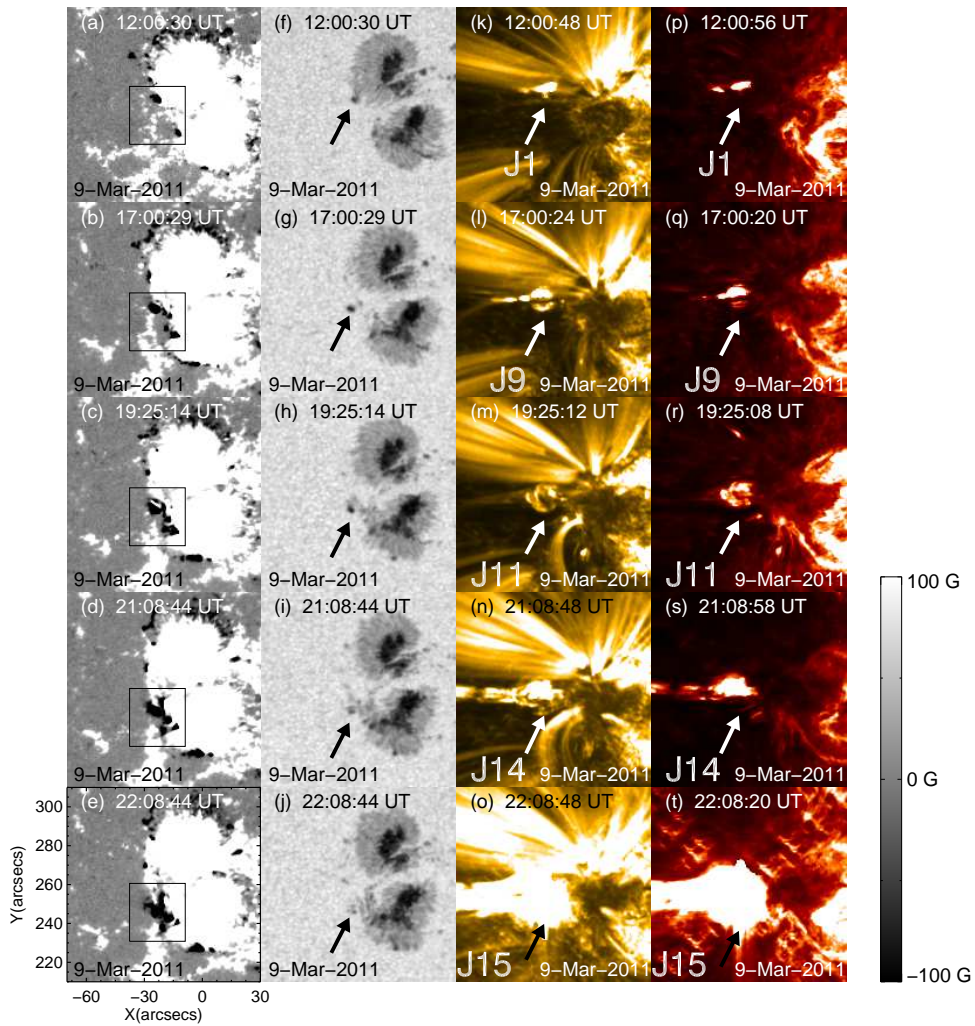


Figure 4. The first column and the second column show the magnetic field and the satellite sunspot evolutions, respectively. The third and fourth column correspond to jet eruptions at 171 Å and 304 Å. The five jets occurred on 09 March 2011. The more jets are shown in the online material (see video1.mpeg in the online journal).

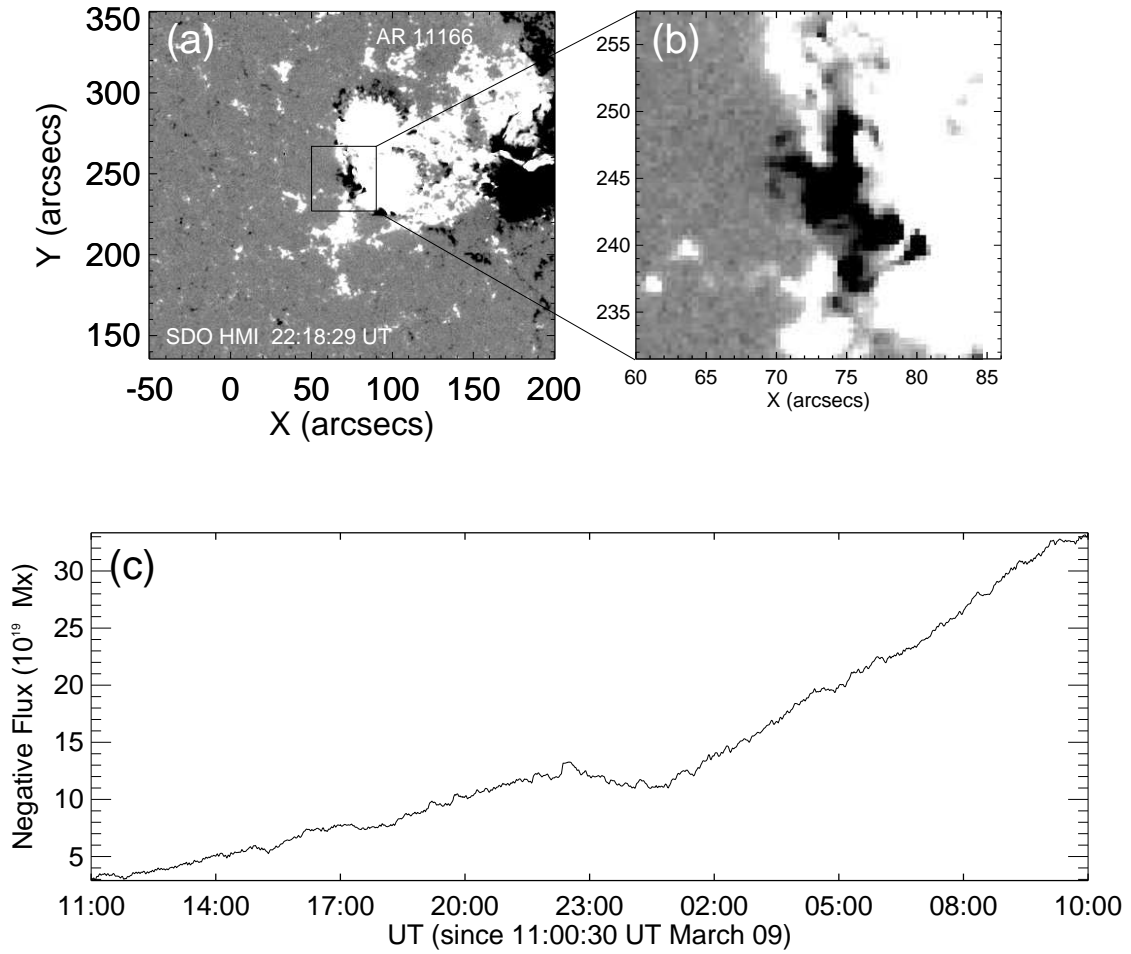


Figure 5. Panel (a) is one HMI LOS magnetogram, with panel (b) consists of a zoomed view of the region marked by a black box in panel (a), highlighting the position of the jet base negative flux. Panels (c) shows the box negative flux variation from 11:00 UT on March 09 to 10:00 UT on March 10.

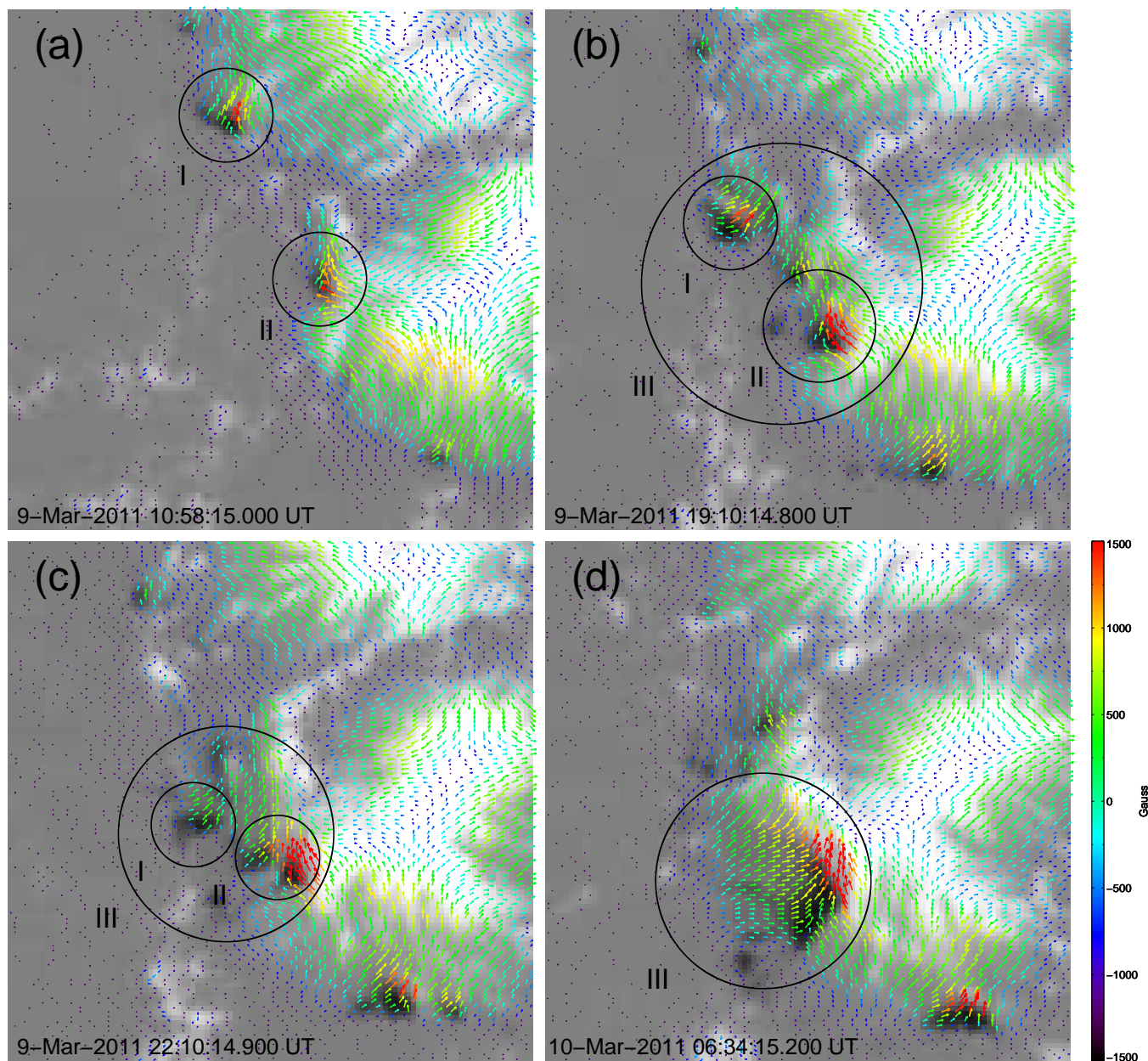


Figure 6. Panels (a)-(d) display the vector magnetic evolution. The Roman numerals “I” and “II” represent satellite sunspot magnetic field and magnetic emergence field, respectively. The “III” displays the mixed and convergence magnetic field region (see video3.mpeg).

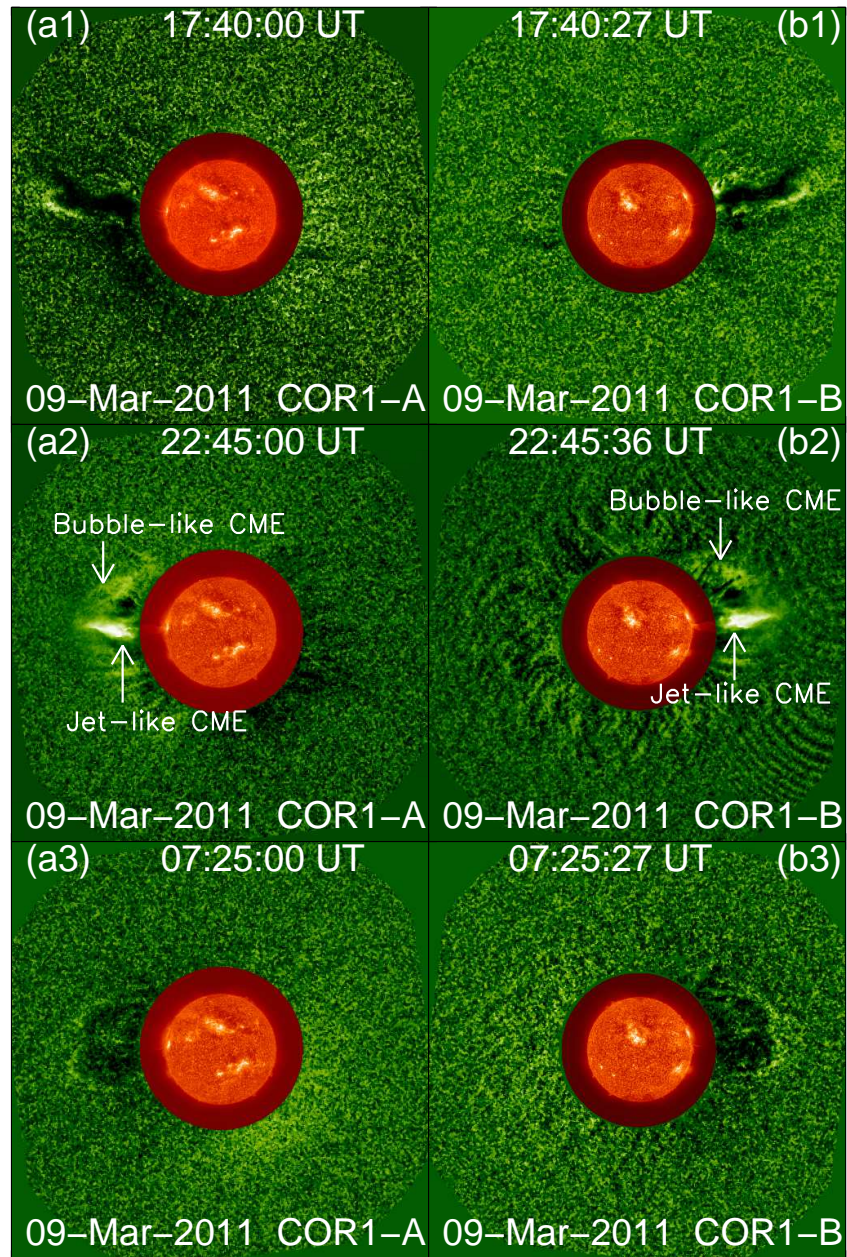


Figure 7. Composite of *STEREO* 304 Å and running difference COR1 Ahead and Behind images showing the three CMEs, which were triggered by J9, J15 and J35, respectively. Panels (a1), (b1) present the first CME event. Panels (a2), (b2) show the double-CME event from the FOVs of *STEREO* COR1 ahead and COR1 behind. The double-CME event has two simultaneous CMEs, namely, the jet-like CME and the bubble-like CME, marked with the white arrows. Panels (a3), (b3) display the third CME event.